Single cell analysis of the aging hypothalamus

Kaitlyn H. Hajdarovic[1], Doudou Yu[2], Lexi-Amber Hassell[3], Shane Evans[4], Nicola Neretti[3,5], Ashley E. Webb[3,5,6,7]*

[1]Graduate program in Neuroscience, Brown University, Providence, RI, 02912, USA.
[2]Graduate program in Molecular Biology, Cell Biology, and Biochemistry, Brown University, Providence, RI 02912, USA.
[3]Department of Molecular Biology, Cell Biology, and Biochemistry, Brown University, Providence, RI 02912, USA.
[4]Graduate program in Computational Biology, Brown University, Providence, RI, 02912, USA.
[5]Center on the Biology of Aging, Brown University, Providence, RI 02912, USA.
[6]Carney Institute for Brain Science, Brown University, Providence, RI 02912, USA.
[7]Center for Translational Neuroscience, Brown University, Providence, RI 02912, USA.

*Correspondence to:
Dr. Ashley Webb
Ashley_Webb@brown.edu
401-863-6840

Key words: Aging, Hypothalamus, Single cell RNA-seq, Brain

ABSTRACT

Alterations in metabolism, sleep patterns, body composition, and hormone status are all key features of aging. The hypothalamus is a well-conserved brain region that controls these homeostatic and survival-related behaviors. Despite the importance of this brain region in healthy aging, little is known about the intrinsic features of hypothalamic aging. Here, we utilize single nuclei RNA-sequencing to assess the transcriptomes of 22,718 hypothalamic nuclei from young and aged female mice. We identify cell type-specific signatures of aging in neurons, astrocytes, and microglia, as well as among the diverse collection of neuronal subtypes in this region. We uncover key changes in cell types critical for metabolic regulation and body composition, as well as in an area of the hypothalamus linked to cognition. In addition, our analysis reveals female-specific changes in sex chromosome regulation in the aging brain. This study identifies critical cell-specific features of the aging hypothalamus in mammals.

43 **INTRODUCTION**

44 While human lifespan has increased dramatically in recent years, improvements in
45 healthspan, the period of life in which a person is disease-free, have been more modest[1].
46 Susceptibility to a host of diseases increases with aging, including diabetes, stroke[2], cancer[3], and
47 neurodegenerative diseases[4]. Aging is accompanied by changes in body composition, including
48 decreased lean muscle mass, loss of bone density, and increased abdominal fat[1]. Concomitant
49 with these changes are alterations in endocrine states, such as decreased sex hormone production,
50 and reduced growth hormone and insulin-like growth factor-I[5]. Endocrine function and
51 homeostatic processes, such as energy homeostasis[6] and release of sex hormones[7], are controlled
52 by neuropeptidergic neurons in the hypothalamus.

53

54 Nutrient sensing is one of several functions of the hypothalamus that implicates this brain
55 region in healthy aging. Specific neuronal subtypes in the hypothalamus respond to circulating
56 cues to organize the response to dietary changes through regulation of energy balance, glucose
57 homeostasis and growth factor secretion. Caloric restriction (CR) is one of the most well-
58 established behavioral interventions that improves lifespan and healthspan in many model
59 organisms[8]. Genetic models that mimic the effects of CR via modulation of energy sensing
60 pathways have revealed the mechanistic underpinnings of lifespan extension. For example, in *C.*
61 *elegans*, the effects of dietary restriction are dependent on the function of neuropeptidergic
62 energy sensing neurons; genetic manipulation of energy sensing genes in those neurons is
63 sufficient to increase longevity[9]. Similarly, lifespan extension in the fruit fly *Drosophila* is
64 dependent on specialized neurons called median neurosecretory cells[10]. In rodents, manipulations
65 to the hypothalamus can also alter lifespan. Specifically, brain-specific over expression of *Sirt1*

66 leads to alterations in the dorsomedial and lateral hypothalamus and increases lifespan[11].
67 Similarly, alteration of immune signaling in the mediobasal hypothalamus affects longevity,
68 where a reduction in immune signaling promotes longevity[12].
69
70 Epigenetic and transcriptional changes are widespread across tissues during aging, including in
71 the brain[13,14]. Key transcriptional factors such as FOXO/DAF-16, NF-κB,, and MYC function as
72 conserved regulators of these networks and have been implicated in aging[12,15,16]. However,
73 despite a great interest in how changes in transcriptional programs affect aging, our
74 understanding of how distinct cellular subtypes change transcriptionally with age remains
75 limited. Investigation of how transcriptional programs change in a cell-type specific manner in
76 the hypothalamus will provide important insight into the aging process across tissues. Recent
77 advances in single-cell RNA-sequencing (RNA-seq) have expanded our understanding of the
78 diverse cell types that comprise the hypothalamus[17–21]. This approach allows the investigation of
79 previously unappreciated transcriptional and functional diversity of this brain region. Here, we
80 use a single nuclei RNA-seq approach to identify aging-associated transcriptional changes across
81 the mouse hypothalamus, thereby capturing the diversity of cell types in this brain region.
82
83 **RESULTS**
84 **Single nuclei sequencing of the aging mouse hypothalamus**
85 We employed single nuclei RNA sequencing (snRNA-seq), which is currently the
86 optimal method for single cell transcriptomic profiling of the diversity of cell types in the adult
87 mammalian brain[22,23]. We isolated nuclei from the hypothalamus of young (3 month) and aged
88 (24 month) mice, with replicate libraries for each age (Figure 1A). After quality filtering, we

89 obtained 22,718 high quality nuclei for analysis: 7862 and 14,856 nuclei from young and aged
90 animals, respectively (Figure S1A). We observed a high correlation between replicates at each
91 age (Figure S1B).
92
93 Clustering analysis with the Louvain algorithm revealed distinct clusters representing the
94 major cell types of the hypothalamus, which we identified based on expression of canonical
95 markers (Figure 1B-D, S1C). For each individual cluster, we identified the top 10 genes that
96 were differentially expressed using the Wilcoxon Rank Sum test (Supplementary Table 1). For
97 example, neurons were defined by expression of *Syt1*, astrocytes defined by *Agt and Gja1*,
98 oligodendrocytes by *Olig1* and *Plp1* expression, and OPCs were identified by expression of
99 *Pdgfra*. The microglia/macrophage cluster was defined by expression of *C1qa* (Figure 1C). Less
100 abundant cell types were also observed, including ependymocytes (ependymal cells; *Ccdc153*),
101 and arachnoid barrier cells (ABC; *Slc47a1*), pericyte/endocytes (*Flt1* and *Clnd5I*) and vascular
102 and leptomeningeal cells (VLMC; *Slc6a13*). We also observed a distinct cluster of tanycytes,
103 which are specific to the hypothalamus and defined by *Rax* expression. Nuclei in these broad
104 categories expressed additional canonical markers associated with their cell type, for example,
105 the astrocyte cluster expressed *Gfap,* further validating the identify of each cluster.
106
107 Cell type diversity is achieved through expression of transcriptional regulators that
108 orchestrate cell type-specific gene expression networks. To identify the regulators responsible for
109 distinct expression networks across cell types in the hypothalamus, we used SCENIC, a
110 regulatory network inference tool. This analysis revealed specific transcriptional regulators of
111 cell identity in this region[24] (Figure 2). Strong cell-type specific signatures emerged for each

112 cluster. Some regulons, such as Foxn2, are strongly enriched across all cell types, while others
113 are unique to one or two cell types. For example, Atf2 is uniquely highly enriched in neurons. In
114 tanycytes, a cell population unique to the hypothalamus, the regulons Foxo1 and Foxo3 are
115 enriched. Tanycytes are considered to be neurogenic, and function in response diet[25,26]. FOXO
116 factors are critical regulators of neural stem cell homeostasis, and FOXOs sit downstream of the
117 insulin/IGF-1 pathway[27]. These data suggest that FOXO factors may be critical regulators of
118 tanycyte response to organismal energy states.
119
120 **Major cell types of the hypothalamus acquire cell type-specific gene expression changes**
121 **with age**
122 We next investigated the changes in gene expression that occur with age in the major cell
123 types of the hypothalamus. As expected, aging was not associated with changes in composition
124 of this brain region, and each major cell type was similarly represented in young and aged mice
125 (Figure 3A). To control for differences in nuclei numbers obtained, we randomly downsampled
126 the aged nuclei and performed differential expression analysis on identical numbers of aged and
127 young nuclei (Figure S2A-C). To gain a global understanding of how gene expression is altered
128 with age, we first performed differential expression analysis using the Model-based Analysis of
129 Single-cell Transcriptomics (MAST)[28,29], treating the data in bulk. Using this approach, we
130 identified 216 and 326 genes that were upregulated and downregulated with age, respectively
131 (padj < 0.05, fold change > 0.1) (Figure 3B, Supplementary Table 3). Intriguingly, highly
132 downregulated genes included *Pmch* and *Oxt*, which encode Pro-melanocyte stimulating
133 hormone and Oxytocin, respectively. Melanocyte stimulating hormone and oxytocin are heavily
134 involved in regulating energy homeostasis[6], which is altered with age[30]. Interestingly, the most

135 upregulated genes included *Xist* and *Tsix*, which are both long non-coding RNAs involved in X
136 chromosome inactivation[31,32].
137
138 Next, we investigated the impact of age on gene expression in each major cell type.
139 Neurons, astrocytes, oligodendrocytes, and microglia showed the greatest numbers of
140 differentially expressed genes with age (Figure 3C, Supplementary Table 4). Analysis of most
141 other cell types also revealed differential expression, though the ability to discern differentially
142 expressed genes was related to the number of nuclei per cluster (Figure S2D). We also performed
143 coefficient of variation analysis on the major cell types and, interestingly, we observed a
144 significant difference between ages, with nearly all types showing in increase with age ($p <$
145 0.001; Wilcoxen test) (Figure 3D). This finding suggests that variability in gene expression
146 increases with age in each cell type, which likely contributes to cellular dysfunction with age.
147
148 To investigate the cellular processes that are altered with age in the different cell types in
149 the hypothalamus, we performed Gene Set Enrichment Analysis (GSEA) using the hallmark
150 gene set[33] (Figure 3E). Interestingly, the neuron sub-cluster had the greatest number of gene sets
151 represented, which included a number of known aging-associated pathways. For example,
152 metabolic pathways such as PI3K/AKT/mTOR, adipogenesis, glycolysis and OxPhos were all
153 under-enriched with age (negative normalized enrichment score). In addition, DNA damage and
154 repair pathways, p53 signaling, and proteostasis were all downregulated in the aged neurons.
155 This analysis also revealed a number of cell type-specific changes with age. For example, among
156 the pathways that were altered with age in astrocytes, some overlapped with the neuronal

157 changes (e.g unfolded protein response and mTORC1 signaling) while others were specific to
158 glia (e.g. coagulation factors, the inflammatory response and NFKB activity).
159
160 **Aged hypothalamic microglia are heterogeneous, representing a progressive aging**
161 **trajectory**
162 Microglia are macrophage-like cells found throughout the brain, and are critical for the
163 immune response, including release of cytokines and chemokines, antigen presentation, and
164 phagocytosis of debris[34]. Recent studies have revealed gene expression changes and microglial
165 activation in the aged brain, which likely contribute to neurodegeneration[34]. Due to the lower
166 frequency of microglia in our dataset, we sought additional strategies to uncover changes with
167 age in these cells. Using Monocle3[35], we performed pseudotemporal ordering of the
168 microglia/macrophage nuclei. The trajectory accurately captures the transition from young to
169 aged nuclei, suggesting a gradual progression toward aging in this cell type (Figure 4A). To
170 identify the gene expression changes across the aging trajectory, we performed Moran's I test
171 (Figure 4B, Supplementary Table 5, Supplementary Table 6). This approach revealed four
172 modules (1, 2, 3, and 7) that have decreased expression along the pseudotime trajectory, and
173 three modules (4-6) with increased expression (Figure 4B-C). We named modules after their
174 most enriched GO term. The modules decreasing in expression along the pseudotime trajectory
175 include terms related to neurotransmitter release, cell migration, cell projection and cytoskeleton
176 makeup, and myelination (Supplementary Table 6). In contrast, the modules increasing with
177 expression across pseudotime include immune response, regulation of cell-cell signaling, and
178 response to immune signals (Supplementary Table 6).
179

180 To gain a deeper understanding of the heterogeneity of microglial aging in the
181 hypothalamus, we examined the top 20 most significant genes for each cluster (q value < 0.05).
182 We visualized expression of genes with high significance in the module and plotted gene
183 expression as a function of pseudotime, and directly comparing young and aged populations
184 (real-time; Figure 4D). This approach reveals that while the young microglia are clustered early
185 in pseudotime (pseudotime 0.0, 0.5 and 1.0), microglial nuclei from aged animals are dispersed
186 throughout pseudotime. Indeed, pseudotime 1.5 and 2.0 are comprised almost entirely of nuclei
187 from aged animals, and expression in these cells varies strongly compared to expression in cells
188 in pseudotime 0.0. Thus, hypothalamic microglia from aged animals have increased
189 heterogeneity representing a progressive aging trajectory, with a subset of microglia retaining a
190 youthful gene expression signature.
191
192 **Age-associated changes in X-inactivation genes is a sexually dimorphic feature of aging**
193 Sex differences in lifespan have been documented in many species, including mice[36]. In
194 addition, interventions that extend life span do so in a sex-specific manner. For example, caloric
195 restriction (CR) is one of the most robustly studied interventions and its effects have been
196 observed from yeast to non-human primates[8]. Like many interventions, CR has sex-specific
197 effects, with restricted females generally living longer than males on the same diet[37,38]. Similarly,
198 the brain-specific *Sirt1* overexpression model results in a larger lifespan increase for females
199 when compared to males[11]. To understand how the female hypothalamus may be uniquely
200 affected by aging, we used female animals in our study.
201

202 Our initial differential expression analysis revealed the unexpected finding that the long
203 non-coding RNA *Xist* is the most highly upregulated gene in the female hypothalamus with age
204 (Figure 3B). Differential expression analysis of each major cell type indicated upregulation of
205 *Xist* with age in astrocytes, neurons, oligodendrocytes, as well as tanycytes (Figure 5A). *Xist* is
206 involved in X chromosome inactivation in females and is encoded on the X-inactivation center
207 (XIC), which harbors additional non-coding RNA genes involved in the same process[39].
208 Intriguingly, we observed age-related upregulation of two of these RNAs in some cell types: *Tsix*
209 and *Ftx*[40] (Figure 5A). We validated the upregulation of *Xist* using whole cell RNA preps from
210 the hypothalamus and investigated other brain regions as well (cerebellum, cortex and olfactory
211 bulb). All regions trended toward increased expression of *Xist* with age, but the strongest
212 upregulation was observed in the hypothalamus (Figure 5B). As expected, we did not detect *Xist*
213 expression in adult male mice, and there was no upregulation of this gene with age in males
214 (Figure 5B).
215
216 The age-associated dysregulation of XIC genes lead us to investigate whether there was
217 an enrichment for expression changes among genes on the X chromosome. Because all three
218 XIC genes assessed were differentially expressed with age in the neuronal cluster (Figure 5A),
219 we focused on neurons. Interestingly, a chi-square analysis indicated that the proportion of
220 upregulated and downregulated genes was not distributed as expected between the X
221 chromosome and autosomes (X^2 = 8.7548, df = 2, p-value = 0.01256). There were more
222 downregulated genes arising from the X chromosome than expected (24 observed, 13.732428
223 expected, standardized residual = 2.9107035). Additionally, there were fewer nonsignificant
224 genes than expected (198 observed, 209.292371 expected, standardized residual = -2.6499813)

225 (Figure 5C). Since the function of *Xist* is to silence gene expression in *cis* on the X, this
226 observation suggests that increased *Xist* with age may contribute to the repression of expression
227 with age across the chromosome.
228
229 Although most genes on the inactive X chromosome are not expressed in females, a small
230 number of genes are well-known to "escape" inactivation, and are expressed from both X
231 chromosomes. In the mouse brain, 14 genes are considered to be X escape genes not silenced by
232 the XIC[41]. This list includes both *Xist* and *Ftx*, which have increased expression with age in our
233 dataset. To determine if increased XIC gene expression with age might be affecting escape
234 genes, we interrogated expression of the other 12 genes in this category. We found that most
235 escape genes were not significantly altered with age in our dataset. In contrast, the X escape
236 genes *Syp* and *Plp1* have decreased expression with age in neurons and oligodendrocytes,
237 respectively. *Ddx3x*, a gene involved in neurodevelopment, showed significantly increased
238 expression with age in astrocytes, although it appears to be expressed at low levels overall
239 (Figure 5D). Together, these data indicate the effect of XIC gene alterations with age may be
240 cell-type specific, and that increased *Xist* expression does not exclusively correlate with the X
241 escape network.
242
243 **Neuronal subtype specific changes during aging**
244 Hypothalamic neurons are highly diverse and function to orchestrate a wide range of
245 processes and behaviors necessary for organismal survival[42]. This diversity of function is
246 accomplished by cell type-specific gene expression programs, with each area of the
247 hypothalamus containing a range of transcriptionally dissimilar neuronal subtypes[17,18,21]. Indeed,

248 even neurons expressing the same neuropeptide gene may comprise functionally distinct
249 subpopulations[43]. To address this complexity, we sub-clustered the neuronal nuclei to identify
250 transcriptionally distinct populations. This analysis revealed 34 transcriptionally distinct clusters
251 (Figure 6A), and broadly separated the nuclei into inhibitory (*Gad1* expressing GABAergic) or
252 excitatory (*Slc17a6* expressing glutamatergic) identity (Figure 6B). The 34 clusters represent
253 both known and undefined neuronal subtypes (see Supplementary Table 7 for markers of cluster
254 identity). To discern the relationship between the clusters, we organized them according to
255 transcriptional similarity using a Cluster Tree analysis (Figure 6C). Neuronal subpopulations
256 from the same hypothalamic nucleus were not necessarily transcriptional neighbors on the cluster
257 tree. For example, even though some AgRP/NPY neurons and POMC neurons may arise from
258 common progenitors[43], the Npy/Agrp (23) and Pomc/Tac2 (25) clusters are not most closely
259 related to one another.
260
261 We next investigated expression of specific neuropeptide genes across the clusters in
262 order to functionally define the distinct neuronal subpopulations (Figure 6D). These clusters
263 generally correspond to known cell types expressing one or two hallmark neuropeptides. As
264 additional insight into neuronal subtype identity, we utilized the SCENIC pipeline to uncover
265 regulons enriched in each cluster[24] (Figure 6E, Supplementary Table 8). For example, Tbx3 is a
266 known regulator of Npy/Agrp cluster (23), and the Tbx3 regulon is active in this cluster in our
267 dataset[44]. Similarly, both POMC and AgRP/NPY neurons are leptin-responsive, and Stat3, the
268 transcriptional regulator of leptin response, is active in both these populations.
269

270 Using this approach, we were able to associate many of these clusters with a known
271 function and location in the hypothalamus, as well as specific changes with age. Similar to our
272 analysis of the whole hypothalamus, we did not detect major changes in neuronal composition
273 with age (Figure 7A). We next performed differential expression on clusters in which there were
274 at least 20 nuclei per condition (Figure 7B, Supplementary Table 9). The number of differentially
275 expressed genes appears to be a function of the number of nuclei per cluster, for example, the
276 Npas3/Gpc cluster (12) which has a large number of nuclei (1923) shows 224 genes
277 downregulated in age and 70 genes upregulated in age. For each cluster, we also performed
278 GSEA using the Hallmark gene set. Interestingly, several neuronal subtypes involved in feeding
279 and energy homeostasis were altered with age. For example, *Ralyl* and *Tenm2* were upregulated
280 in the Npy/Agrp cluster (23). In the Pomc/Tac2 cluster (25), *Plod1* and *Cxcl12* were
281 downregulated, and *Epha6, Xist, B3galt1, Lingo2*, and *Sgcz* were upregulated. Pathways altered
282 in this cluster with age include adipogenesis, DNA repair, oxidative phosphorylation, the
283 unfolded protein response, and UV response down (Figure 7C). Thus, for the first time, our
284 dataset links neuron-specific gene expression changes in the hypothalamus with key features of
285 organismal aging, such as weight and metabolic changes.
286
287 Based on expression of specific peptides and transcription factors, the
288 Dgkb/B230323A14Rik cluster (7) is likely made up of cells of the medial mammillary nucleus.
289 This region is notable because unlike most areas of the hypothalamus, this region is involved in
290 memory via connections with the hippocampus[45]. Strikingly, this cluster is highly dysregulated
291 with age, with 65 downregulated and 31 upregulated genes. This gene set is enriched for changes
292 in adipogenesis, mTORC1 signaling, OxPhos, DNA damage (UV response down), and

293 xenobiotic metabolism. The identification of changes in this brain region is significant, as they
294 may contribute to cognitive impairments with age.

295 **DISCUSSION**

296 In this work, we used single nuclei RNA-seq to identify the age-associated transcriptional
297 changes in the mouse hypothalamus. This brain region is critical for the regulation of
298 physiological homeostasis, including sleep, circadian rhythms, feeding, and metabolism. These
299 functions are well known to be disrupted during aging, and our findings implicate widespread
300 transcriptional changes concomitant with physiological changes.
301
302 Our approach successfully captured the major cell types in the brain, as well as
303 hypothalamus-specific cell-types such as tanycytes. We found that cellular subtypes in this
304 region acquire distinct aging signatures, and discovered that increased transcriptional
305 heterogeneity is a common feature across all cell types with age. Consistent with our findings,
306 age-related transcriptional alterations have been observed in aging human brains[46], and increased
307 transcriptional noise is thought to be a hallmark of aging[47]. Our finding that different neuronal
308 subtypes have distinct aging signatures is consistent with recent reports identifying differential
309 susceptibility to neurodegeneration[48]. Identification of the transcriptional signatures involved
310 may pave the way for therapeutics targeted at subpopulations most susceptible to dysregulation
311 with age. In addition, analysis of cell types arising from the arcuate nucleus illustrate intriguing
312 cell-type specific differences in populations responsible for nutrient sensing. For example,
313 despite the importance of AgRP/NPY neurons in initiating feeding in steady state animals[49], the
314 Npy/Agrp cluster (23) is relatively unaffected by age. In contrast, the Pomc/Tac2 cluster (25)
315 gene set is enriched for changes in DNA repair and the unfolded protein response, among others.

316 While these two cell populations have complementary functions in steady state, POMC neurons
317 seem to be uniquely affected by aging. Interestingly, upregulation of the unfolded protein
318 response has been linked to improved protection against diet-induced obesity[50]. Thus, the
319 downregulation of the unfolded protein response pathway with age in these cells may represent a
320 mechanism underlying body composition changes that occur with age.
321
322 We observed striking changes in the microglial population with age. Microglia are
323 resident immune cells in the brain, and previous research has shown that microglia-mediated
324 inflammation in the hypothalamus can affect lifespan[12]. By utilizing trajectory inference
325 analysis, we uncovered an aging trajectory among microglia in the aged brain. While some
326 microglia retain features of young cells, the population shows a progression toward an aged
327 phenotype based on distinct gene expression modules. Interestingly, modules of immune genes
328 were some of the most changed throughout pseudotime. Module 2, which contains GO
329 categories related to leukocyte migration, cell chemotaxis, and cell-cell adhesion, was among the
330 most downregulated with pesudeotime. In contrast, Module 4, which also contains GO categories
331 related to immune function, was highly upregulated with pseudotime. Together, these data
332 indicate that the aged hypothalamus harbors a heterogeneous population of microglia comprising
333 an aging trajectory.
334
335 Sex differences in aging have been observed across taxa, including in mice[51,52]. In
336 mammals, females generally live longer than males[53], and many aging interventions such as CR,
337 are more effective in females[11,37]. In addition, the sexually dimorphic response to aging
338 interventions appears to be a conserved phenomenon, with female *Drosophila* responding more

339 strongly to dietary restriction paradigms than males[54], and hermaphroditic *C. elegans* responding
340 more strongly to DR than males[55]. In mice, males and females differ in regards to sex
341 chromosome content (males are XY and females are XX) and the presence of gonadal hormones
342 such as higher androgens in males and estrogens in females. Interestingly, X chromosome
343 content has been linked to longevity, and the presence of two X chromosome contributes to
344 increased longevity regardless of hormonal status[56]. This work was performed in the four core
345 genomes mouse line, in which the *Sry* gene (which induced testes development) exists on an
346 autosome rather than the Y chromosome, allowing for chromosomal sex to be disambiguated
347 from gonadal sex/hormone status. In our study, we uncover a potential mechanism by which the
348 X chromosome affects aging. We observed widespread upregulation of *Xist* in aged female
349 animals, as well as upregulation of other XIC genes including *Tsix* and *Ftx*. Intriguingly, this
350 increased expression was highly prominent in neurons, although upregulation of *Xist* in was
351 observed in oligodendrocytes, astrocytes, and tanycytes as well. Together, our findings reveal a
352 novel feature of aging in females. Moreover, this work suggests that that understanding the
353 mechanisms and consequences of *Xist* upregulation in aging may provide novel insight into sex
354 differences in aging.
355
356 In summary, our study reveals the major transcriptional features of hypothalamic aging.
357 We observed transcriptional variation across cell types, cell-type specific aging signatures, and
358 novel features of aging in females. Understanding how individual populations of cells in this
359 region contribute to overall loss of homeostasis with age will be vital to identifying treatments
360 for aging and age-related disease.
361

362

363 **METHODS**

364 *Animals*

365 Young (3 month) and aged (24 month) C57/Bl6 female mice were obtained from the
366 National Institute on Aging. Mice were housed and used according to protocols approved by
367 Brown University and in accordance with institutional and national guidelines.

368

369 *Single-cell RNA sequencing*

370 Two whole hypothalamuses were pooled into each biological replicate, for a total of two
371 replicates for the young and aged conditions. Nuclei extraction was performing using the Nuclei
372 Isolation Kit: Nuclei PURE Prep Kit (Millipore Sigma) according to the manufacturer's
373 instructions with the following modifications: for each sample, two hypothalamuses were
374 dissected out of the animals and rinsed in cold PBS. Tissue was transferred using a transfer
375 pipette into a refrigerated Dounce homogenizer with 5 mL of lysis solution following kit
376 instructions. Tissue was homogenized with the Dounce B and the lysate was transferred into a 15
377 mL falcon tube through a 40-micron filter. The sucrose purification step was performed with the
378 following modifications: half the volume of all reagents was used to account for the small tissue
379 sample sizes, an SW34 rotor was used, and samples were spun for 45 minutes at 30,000 X g
380 (13,000 rpm) at 4 °C. Nuclei were counted using a hemocytometer, and 5000 cells per sample
381 were loaded onto the Chromium Single Cell 3′ Chip (10x Genomics) and processed with the
382 Chromium Controller (10x Genomics). Libraries were prepared using the Chromium Single Cell
383 3′ Library & Gel Bead kit v2 according to manufacturer's instructions. Samples were sequenced
384 at GENEWIZ, Inc on an Illumina HiSeq, with a target of 50,000 reads per sample. The Aged 1

385 and Young 2 samples underwent an additional round of sequencing to obtain sufficient read
386 depth.
387
388 *Quality control, data processing and analysis*
389 Demultiplexing and sequence alignment to a custom pre-mRNA transcriptome (mm10-
390 3.0.0) were performed using the CellRanger (version 3.0.2) software from 10x Genomics. The
391 resulting feature-barcode matrices were read into R, excluding any nuclei expressing fewer than
392 200 genes, and any gene expressed in fewer than three nuclei.
393
394 Filtering and visualization were performed using Seurat_3.2.3 in R (4.0.3). For quality
395 control, cells with fewer than 200 or more than 3000 features were filtered out. Similarly, cells
396 with more than 10% mitochondrial mapping were removed, resulting in 14,856 nuclei in the
397 aged condition, and 7862 nuclei in the young condition. Integration of the datasets was
398 performed using the IntegrateData function with default settings. The number of cells, unique
399 molecular identifiers, and unique genes per cluster are reported in Supplementary Figure 1C. To
400 assign identities to clusters, the FindAllMarkers() command with default parameters was used.
401 This finds the top genes that define a cluster identity. We named each cluster using the top 2
402 genes to come out of the FindAllMarkers() analysis. This function uses the Wilcoxon Rank Sum
403 test identify the top 10 differentially expressed genes in cell-type specific clusters, with a log fold
404 change threshold of 0.25.
405
406 In order to ensure similar cell counts per condition, data were downsampled by randomly
407 selecting cells from each cluster using the sample() function in R. Differential expression was

408 performed using MAST(1.16.0)[28]. Genes were considered significant if the adjusted p-value was
409 less than 0.05, and the log2 fold change was greater than 0.1 or less than -0.1.
410
411 *Gene Set Enrichment Analysis*
412 Gene Set Enrichment Analysis was performed using the fgsea package (Release 3.12)[57]
413 using the Hallmark gene set list (version 7.2.)[33]. Gene sets were considered to be enriched if the
414 adjusted p value was less than 0.1. Conversions between mouse and human annotation was
415 performed using biomaRt (2.46.0).
416
417 *Trajectory inference and analysis using Monocle3*
418 The trajectory inference tool Monocle3[35] (https://github.com/cole-trapnell-lab/monocle3)
419 was used to infer the aging process for the microglia cluster (n = 761 cells) generated in Seurat.
420 The microglia cluster was subsetted and the root of the trajectory was programmatically
421 specified using the node that was most enriched with young cells. Spatially differential
422 expression analysis along the trajectory was performed with Moran's I test in Monocle3 using
423 the downsampled microglia data (n = 448 cells), and selected genes with $q < 0.05$ as trajectory-
424 dependent genes. The set of genes were grouped into seven modules using find_gene_modules()
425 to run UMAP on these genes and group them into modules by Louvain community analysis
426 (Supplementary Table 6).
427
428 *Functional enrichment analysis*
429 The g:Profiler g:GOSt tool was applied to perform the functional enrichment analysis of
430 939 genes in individual microglia modules, and to identify statistically significant enriched terms

431 (adjusted $p < 0.05$ with Benjamini-Hochberg correction) for individual modules (Supplementary
432 Table 5). Seven modules were identified: Module 1 (19 terms), module 2 (25 terms), module 3
433 (26 terms), module 4 (202 terms), module 5 (11 terms), module 6 (13 terms), module 7 (6 terms).
434 The 939 genes were treated as unordered queries, and statistical tests were applied in a domain
435 scope of annotated genes, choosing terms sized from 4 to 500 genes in sources including GO
436 molecular function, GO cellular component, GO biological process, KEGG, Reactome, and
437 WikiPathways. The top GO biological process term was used to name individual modules.
438
439 ***Single-cell gene regulatory network analysis using pySCENIC***
440

441 We performed GRN analysis with pySCENIC v0.10.4[24] using the Singularity v3.6.1 image.
442 We first converted the Seurat object (DefaultAssay: RNA, i.e. raw counts without normalization)
443 with loomR v0.2.1.9 and export into a loom file for the GRN inference. In the GRN
444 inference, for the downsampled all-cell data (n=15445 cells), we filtered out genes that are
445 detected in less than 300 cells with Scanpy v1.4.4, resulting in 11574 genes in total; for the
446 downsampled neuron data (n= 8846 cells), we used all genes (22054 genes). We performed 100
447 runs on both datasets. Only regulons that recurred at least 80% were retained, along with target
448 genes that were predicted to recur at least 80% if the regulon recurred 100 times, and all target
449 genes for regulons that recurred between 80 and 100 times[58]. After filtering, we identified 216
450 motif regulons for all-cell dataset, and 285 motif regulons for neurons. The regulon activity was
451 quantified by AUCell with AUCell_calcAUC in AUCell R package v1.8.0, R/3.6.3. To
452 understand if a regulon is active or not in a specific cell type, we created a binary regulon
453 activity matrix of the filtered regulons with binarize function in pyscenic.binarization and
454 visualized in R. For the regulon specificity score (RSS), we use the regulon_specificity_scores

455 from pyscenic.rss[59]. The RSS is calculated for each cell type separately, and top 5 regions for

456 each cell type are shown in red.ref.

457

458 *Data and code availability*

459 Raw single nuclei RNA sequencing deposited at GEO accession XYZ. Code available at

460 https://github.com/Webb-Laboratory/single_cell_analysis.

461

462 *RT-qPCR*

463 Hypothalamus, olfactory bulb, cerebellum, and cortex were dissected in cold PBS from

464 the brains of 3 month old and 24 month old C57Bl/6 mice (n=6, 3 male and 3 female for each

465 age) and snap frozen in liquid nitrogen. RNA was purified using the Qiagen RNeasy Lipid

466 Tissue Mini Kit (Qiagen #74804). cDNA was generated using 500 ng of RNA and the High-

467 Capacity Reverse Transcription Kit (Applied Biosystems #4374966). A negative control (-RT)

468 for each sample was also generated by excluding the Multiscribe Reverse Transcriptase

469 component of the reaction. qPCR reactions were completed using the PowerUp™ SYBR ™

470 Green Master Mix (Invitrogen #A25918). Stock primers were diluted to 10 µM in sterile water,

471 and cDNA was diluted 1:5 in sterile water. Expression levels of the genes of interest (see table

472 below) were quantified using a ViiA 7 Real Time PCR System with QuantStudio software. *Actin*

473 was used as a housekeeping gene for normalization. Each sample, water control, and -RT control

474 sample was run in triplicate for each primer set. CT values were normalized to *Actin*, and ΔCT

475 values were plotted as $2^{-\Delta CT}$. Technical replicates were averaged per biological replicate.

476

Gene	F sequence	R sequence

Actin	TGTTACCAACTGGGACGACA	CTCTCAGCTGTGGTGGTGAA
Xist	GGTTCTCTCTCCAGAAGCTAGGAAG	TGGTAGATGGCATTGTGTATTATATGG

477

478

479 **SUPPLEMENTARY MATERIAL**

480 Supplementary Table 1. Markers for hypothalamic cell clusters.
481 Supplementary Table 2. Binarized regulons for hypothalamic cell clusters.
482 Supplementary Table 3. Results of differential expression analysis for all nuclei.
483 Supplementary Table 4. Differential expression analysis of individual cell types.
484 Supplementary Table 5. Results of Moran's I Test.
485 Supplementary Table 6. Gene modules from monocle analysis.
486 Supplementary Table 7. Cluster markers for neuronal subtypes.
487 Supplementary Table 8. Regulon specificity scores for each neuronal cluster.
488 Supplementary Table 9. Results of differential expression for neuronal subtypes.

489

490

491

492

493

Figure 1.

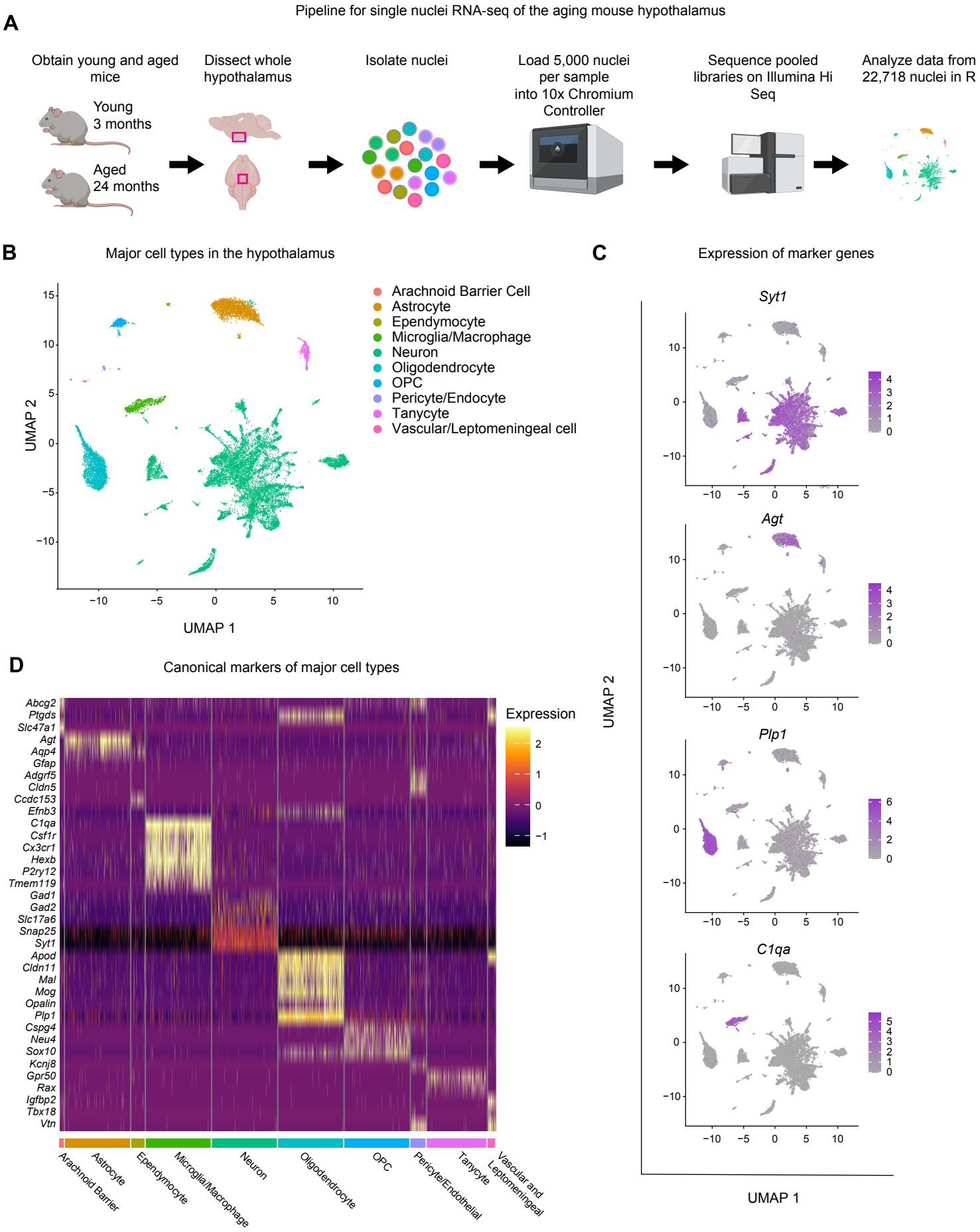
A
Pipeline for single nuclei RNA-seq of the aging mouse hypothalamus
Obtain young and aged mice
Young 3 months
Aged 24 months
Dissect whole hypothalamus
Isolate nuclei
Load 5,000 nuclei per sample into 10x Chromium Controller
Sequence pooled libraries on Illumina Hi Seq
Analyze data from 22,718 nuclei in R
B
Major cell types in the hypothalamus
Arachnoid Barrier Cell
Astrocyte
Ependymocyte
Microglia/Macrophage
Neuron
Oligodendrocyte
OPC
Pericyte/Endocyte
Tanycyte
Vascular/Leptomeningeal cell
UMAP 2
UMAP 1
C
Expression of marker genes
Syt1
Agt
Plp1
C1qa
UMAP 2
UMAP 1
D
Canonical markers of major cell types
Abcg2
Ptgds
Slc47a1
Agt
Aqp4
Gfap
Adgrf5
Cldn5
Ccdc153
Efnb3
C1qa
Csf1r
Cx3cr1
Hexb
P2ry12
Tmem119
Gad1
Gad2
Slc17a6
Snap25
Syt1
Apod
Cldn11
Mal
Mog
Opalin
Plp1
Cspg4
Neu4
Sox10
Kcnj8
Gpr50
Rax
Igfbp2
Tbx18
Vtn
Expression
Arachnoid Barrier
Astrocyte
Ependymocyte
Microglia/Macrophage
Neuron
Oligodendrocyte
OPC
Pericyte/Endothelial
Tanycyte
Vascular and Leptomeningeal

630 **FIGURE LEGENDS**

631 **Figure 1. Single-nuclei analysis of the hypothalamus.** A) Schematic detailing the experimental
632 workflow from dissection through analysis. n = 2 replicated per age. B) Uniform Manifold
633 Approximation and Projection (UMAP) plot of all 22,718 nuclei used for analysis. Clustering
634 analysis revealed 10 broad categories of cell type identity. C) UMAP plots of all nuclei labeled
635 for expression of cell type-specific markers. *Syt1*, neurons; *Agt*, astrocytes; *Plp1*,
636 oligodendrocytes; *C1qa*, microglia/macrophages. Color scale indicates level of gene expression.
637 D) Heatmap highlighting expression of cell type markers in each cluster, a maximum of 500
638 nuclei per cluster are displayed. E) RSS scores for representative subclusters. Top 5 regulons in
639 red.

640

641

642

643

644

645

646

647

648

649

650

651

Figure 2.

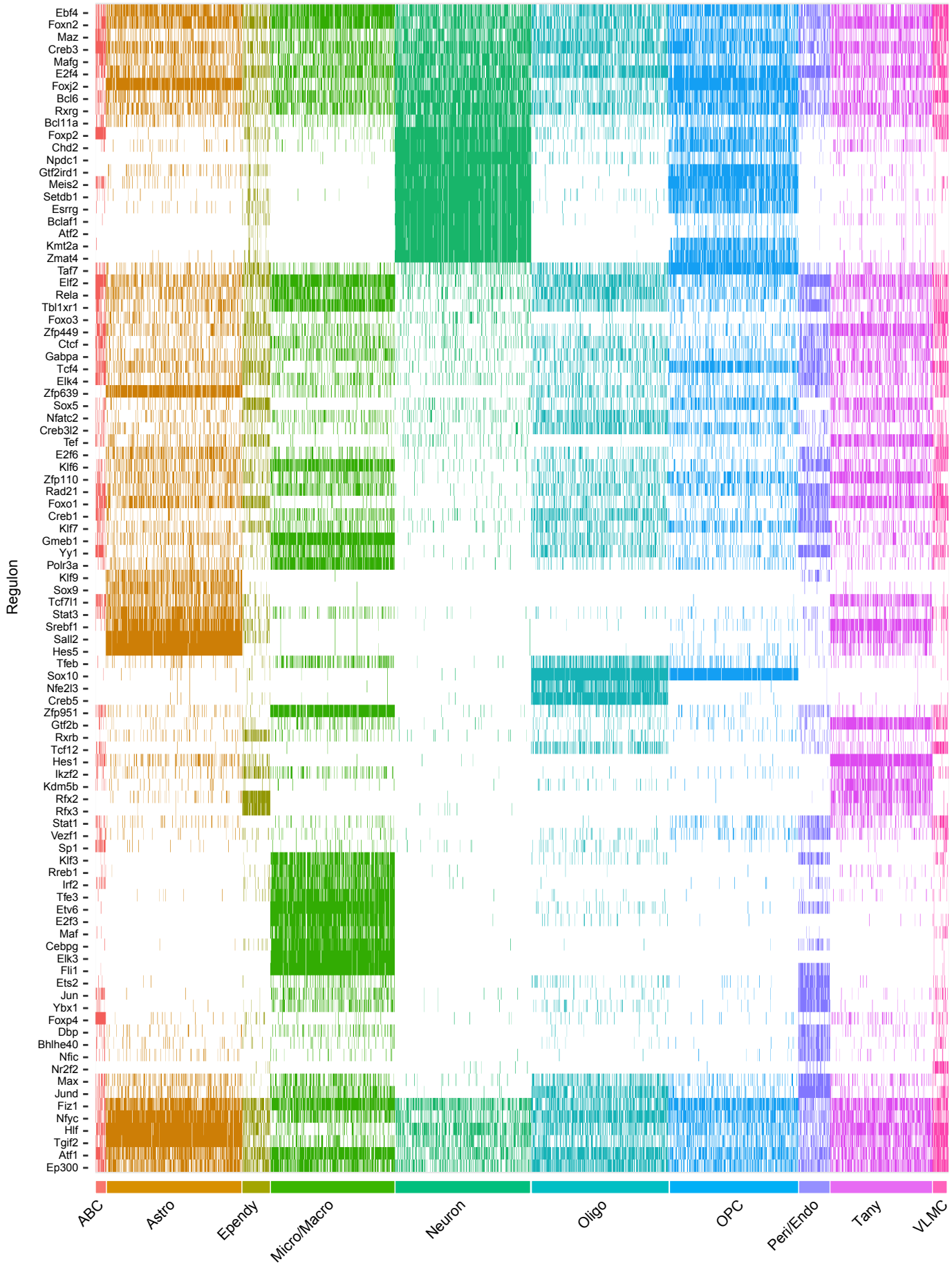
Regulon
Ebf4
Foxn2
Maz
Creb3
Mafg
E2f4
Foxj2
Bcl6
Rxrg
Bcl11a
Foxp2
Chd2
Npdc1
Gtf2ird1
Meis2
Setdb1
Esrrg
Bclaf1
Atf2
Kmt2a
Zmat4
Taf7
Elf2
Rela
Tbl1xr1
Foxo3
Zfp449
Ctcf
Gabpa
Tcf4
Elk4
Zfp639
Sox5
Nfatc2
Creb3l2
Tef
E2f6
Klf6
Zfp110
Rad21
Foxo1
Creb1
Klf7
Gmeb1
Yy1
Polr3a
Klf9
Sox9
Tcf7l1
Stat3
Srebf1
Sall2
Hes5
Tfeb
Sox10
Nfe2l3
Creb5
Zfp951
Gtf2b
Rxrb
Tcf12
Hes1
Ikzf2
Kdm5b
Rfx2
Rfx3
Stat1
Vezf1
Sp1
Klf3
Rreb1
Irf2
Tfe3
Etv6
E2f3
Maf
Cebpg
Elk3
Fli1
Ets2
Jun
Ybx1
Foxp4
Dbp
Bhlhe40
Nfic
Nr2f2
Max
Jund
Fiz1
Nfyc
Hlf
Tgif2
Atf1
Ep300
ABC
Astro
Ependy
Micro/Macro
Neuron
Oligo
OPC
Peri/Endo
Tany
VLMC

652 **Figure 2. Gene regulatory network reconstruction for cellular subtypes.** A) Binarized
653 regulon activity for each regulon in a given cell. Top 20 most expressed regulons per cluster
654 shown. Maximum 500 cells per cluster shown. Color indicates a regulon is "on" in a given cell.
655
656
657
658
659
660
661
662
663
664
665
666
667
668
669
670
671
672
673

Figure 3.

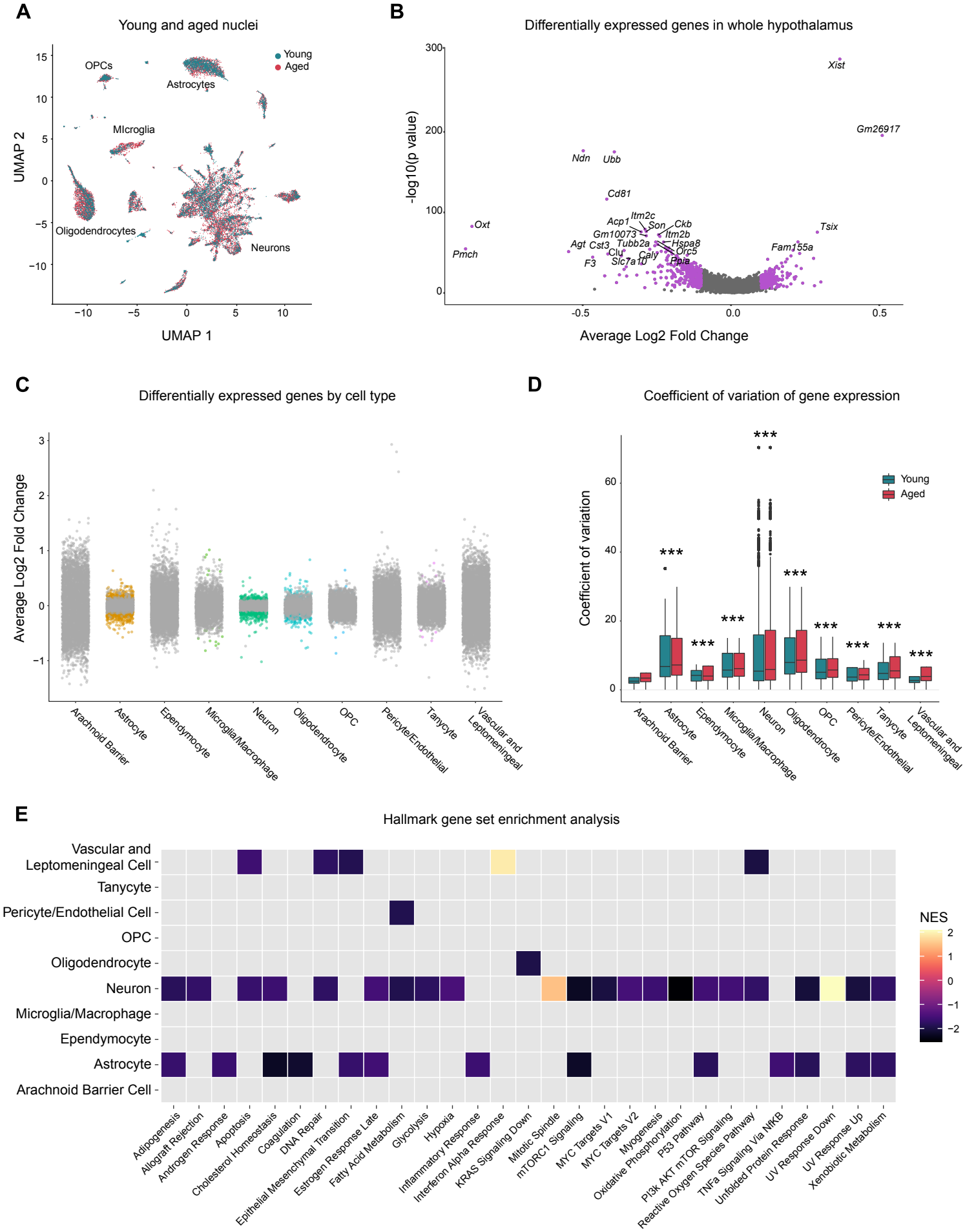
A
Young and aged nuclei
Young
Aged
OPCs
Astrocytes
MIcroglia
Oligodendrocytes
Neurons
UMAP 2
UMAP 1
B
Differentially expressed genes in whole hypothalamus
-log10(p value)
Average Log2 Fold Change
Xist
Gm26917
Ndn
Ubb
Cd81
Oxt
Pmch
Tsix
Fam155a
C
Differentially expressed genes by cell type
Average Log2 Fold Change
Arachnoid Barrier
Astrocyte
Ependymocyte
Microglia/Macrophage
Neuron
Oligodendrocyte
OPC
Pericyte/Endothelial
Tanycyte
Vascular and Leptomeningeal
D
Coefficient of variation of gene expression
Coefficient of variation
Young
Aged
E
Hallmark gene set enrichment analysis
Vascular and Leptomeningeal Cell
Tanycyte
Pericyte/Endothelial Cell
OPC
Oligodendrocyte
Neuron
Microglia/Macrophage
Ependymocyte
Astrocyte
Arachnoid Barrier Cell
Adipogenesis
Allograft Rejection
Androgen Response
Apoptosis
Cholesterol Homeostasis
Coagulation
DNA Repair
Epithelial Mesenchymal Transition
Estrogen Response Late
Fatty Acid Metabolism
Glycolysis
Hypoxia
Inflammatory Response
Interferon Alpha Response
KRAS Signaling Down
Mitotic Spindle
mTORC1 Signaling
MYC Targets V1
MYC Targets V2
Myogenesis
Oxidative Phosphorylation
P53 Pathway
PI3k AKT mTOR Signaling
Reactive Oxygen Species Pathway
TNFa Signaling Via NfKB
Unfolded Protein Response
UV Response Down
UV Response Up
Xenobiotic Metabolism
NES

674 **Figure 3. The aging hypothalamus harbors cell type-specific transcriptional changes.** A)
675 UMAP of the 22,718 nuclei analyzed, color indicates age. B) Volcano plot showing overall
676 differential expression of genes between all young and aged nuclei. Significant genes in purple
677 (adjusted p value < 0.05, FC > 0.1). C) Strip plot showing DE genes per cell type. Significant
678 genes (adjusted p value < 0.05, FC > 0.1, MAST analysis) in color, nonsignificant genes are in
679 gray. D) Coefficient of variation analysis for each cellular subtype. In all subtypes the CV is
680 significantly higher in the aged condition (two sided Wilcoxen Test with Bonferonni correction,
681 ***adjusted p value < 0.001). E) Heatmap showing GSEA enrichment analysis for Hallmark
682 terms. Color indicates normalized enrichment score. Significant gene sets calculated as adjusted
683 p value < 0.1.
684
685
686
687
688
689
690
691
692
693
694
695
696

Figure 4.

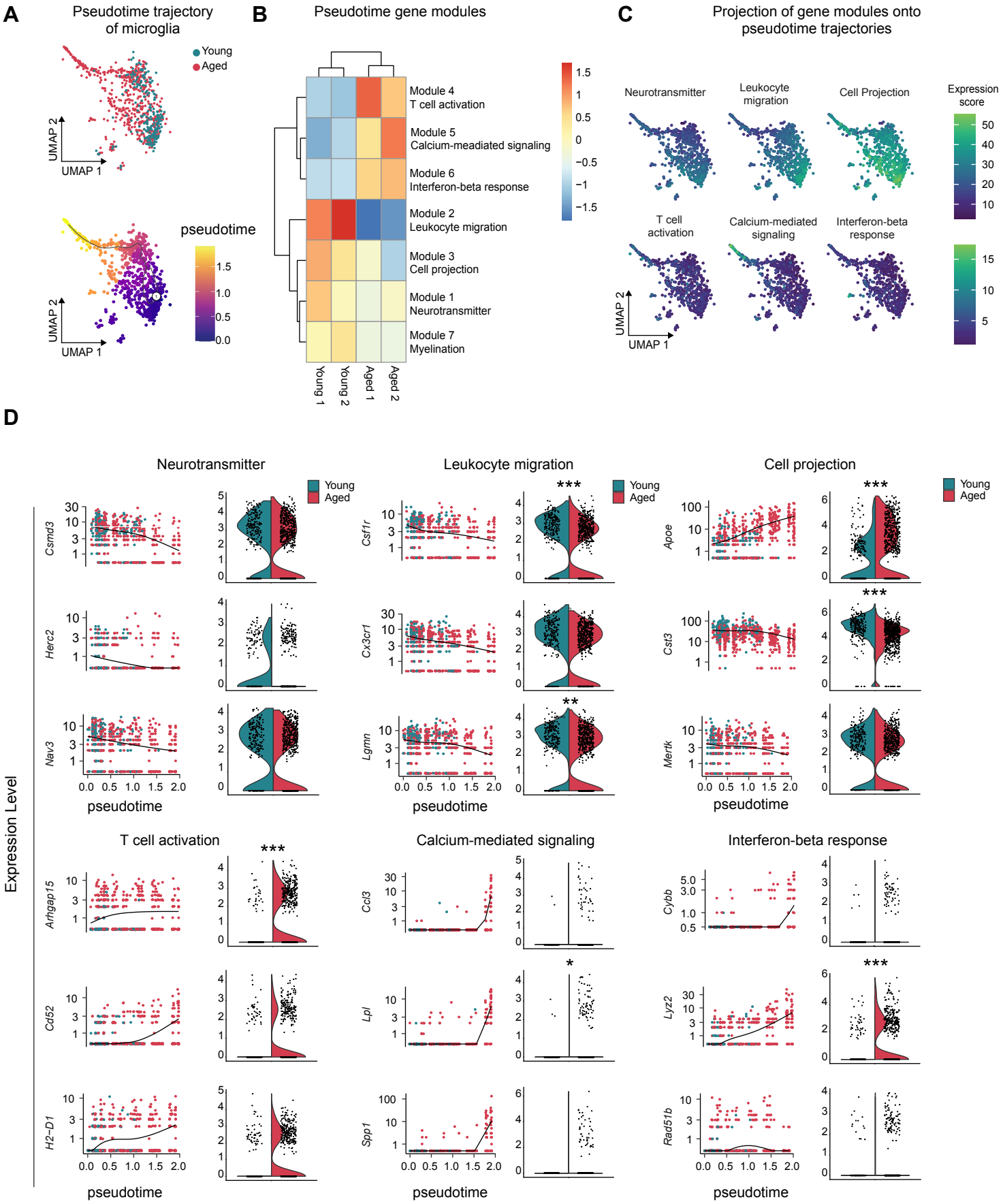
A
Pseudotime trajectory of microglia
Young
Aged
UMAP 2
UMAP 1
pseudotime
1.5
1.0
0.5
0.0
B
Pseudotime gene modules
Module 4
T cell activation
Module 5
Calcium-meadiated signaling
Module 6
Interferon-beta response
Module 2
Leukocyte migration
Module 3
Cell projection
Module 1
Neurotransmitter
Module 7
Myelination
Young 1
Young 2
Aged 1
Aged 2
1.5
1
0.5
0
−0.5
−1
−1.5
C
Projection of gene modules onto pseudotime trajectories
Neurotransmitter
Leukocyte migration
Cell Projection
T cell activation
Calcium-mediated signaling
Interferon-beta response
Expression score
50
40
30
20
10
15
10
5
UMAP 2
UMAP 1
D
Neurotransmitter
Leukocyte migration
Cell projection
T cell activation
Calcium-mediated signaling
Interferon-beta response
Young
Aged
Expression Level
Csmd3
Herc2
Nav3
Csf1r
Cx3cr1
Lgmn
Apoe
Cst3
Mertk
Arhgap15
Cd52
H2-D1
Ccl3
Lpl
Spp1
Cybb
Lyz2
Rad51b
***
**
*
pseudotime

697 **Figure 4. Trajectory analysis of aging hypothalamic microglia.** A) Monocle3 pseudotemporal
698 ordering of the microglia/macrophage cluster (n = 761 cells). Cells are colored by age (top) and
699 pseudotime (bottom). The number in the circle indicates the pseudotime start point. B) Heatmap
700 showing modules of spatially restricted genes in the microglia cluster after downsampling (n =
701 448 cells). In total, 939 genes were clustered by hierarchical clustering. The genes were grouped
702 into seven modules after dimension reduction and community detection. Modules are named by
703 the most significantly enriched Gene Ontology (GO) terms, biological process, for module-
704 specific genes using g:Profiler (adjusted $p < 0.05$ with Benjamini-Hochberg correction). C)
705 Projection of modules' aggregate expression onto the UMAP plot for microglia cluster (n = 761
706 cells). Genes in modules 1-3 have decreased expression along the pseudotime trajectory. Genes
707 in modules 4-6 have increased expression along the pseudotime trajectory. D) Left: kinetics plot
708 showing the relative expression of representative genes for modules 1-6. The lines approximate
709 expression along the trajectory using polynomial regressions. Right: violin plots of gene
710 expression using Seurat. Differential expression performed using MAST on non-downsampled
711 data (* , adjusted p value < 0.05, ***, adjusted p value < 0.001).
712
713
714
715
716
717
718

Figure 5

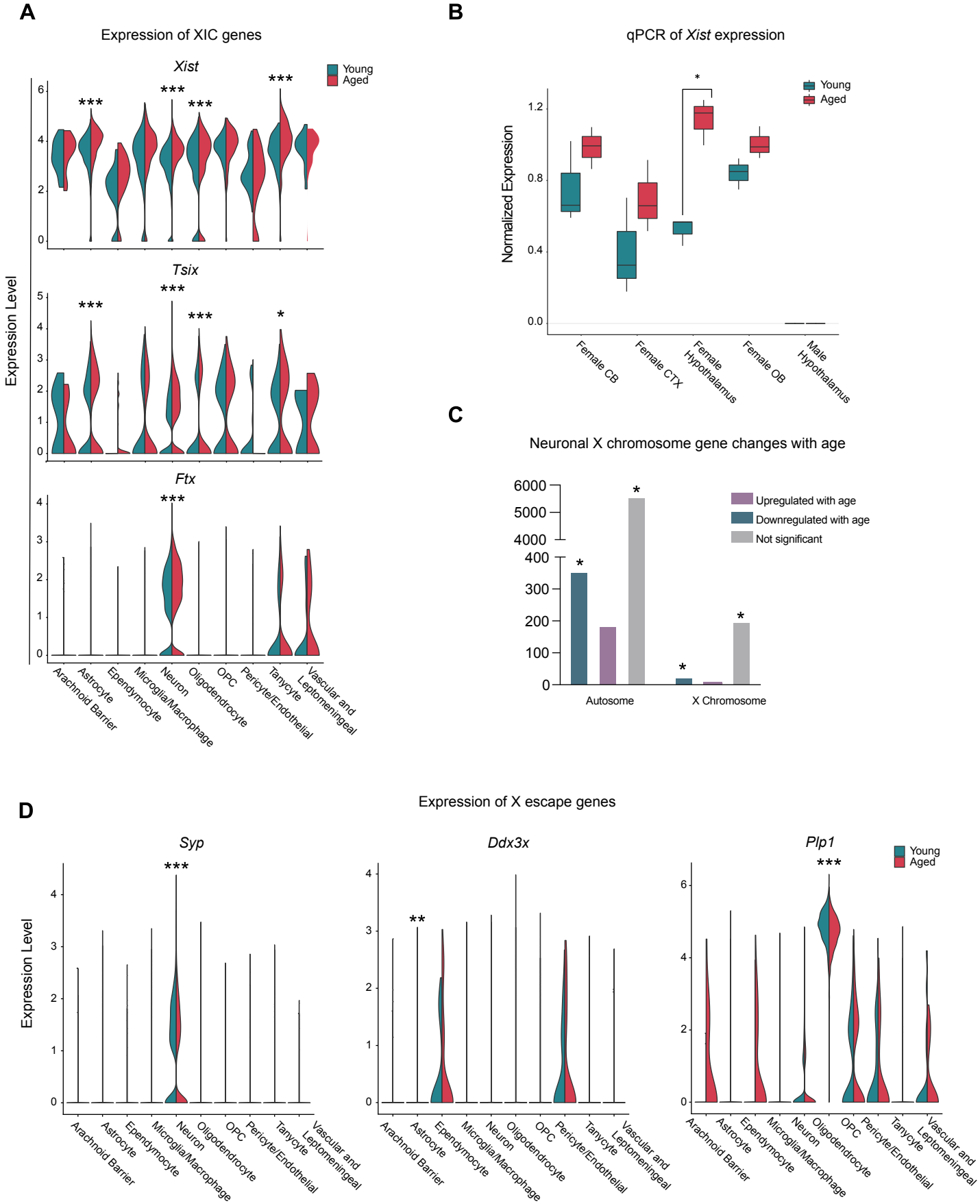
A
Expression of XIC genes
Xist
Tsix
Ftx
Young
Aged
Expression Level
Arachnoid Barrier
Astrocyte
Ependymocyte
Microglia/Macrophage
Neuron
Oligodendrocyte
OPC
Pericyte/Endothelial
Tanycyte
Vascular and Leptomeningeal
B
qPCR of Xist expression
Normalized Expression
Female CB
Female CTX
Female Hypothalamus
Female OB
Male Hypothalamus
C
Neuronal X chromosome gene changes with age
Upregulated with age
Downregulated with age
Not significant
Autosome
X Chromosome
D
Expression of X escape genes
Syp
Ddx3x
Plp1

719 **Figure 5. *Xist* upregulation is a feature of the aged female hypothalamus**. A) Expression of
720 genes involved in X chromosome inactivation by age and cell type. Differential expression
721 between young and aged samples was calculated using MAST (* , adjusted p value < 0.05, ***,
722 adjusted p value < 0.001). B) RT-qPCR of *Xist* expression in specific brain regions. *Xist*
723 expression is significantly higher in the hypothalamus (two sided t test, t = 7.06, df = 3.25, n = 3
724 per age group, *p adjusted = 0.0179, Bonferroni correction). C) Comparison of the number of
725 upregulated, downregulated, and non-significant genes arising from the X chromosome or
726 autosomes in (X^2 = 8.7548, df = 2, p-value = 0.01256). D) Violin plots of known X escape genes.
727 Differential expression between young and aged samples was calculated using MAST (* ,
728 adjusted p value < 0.05, **, adjusted p value < 0.01, ***, adjusted p value < 0.001).
729
730
731
732
733
734
735
736
737
738
739
740

Figure 6.

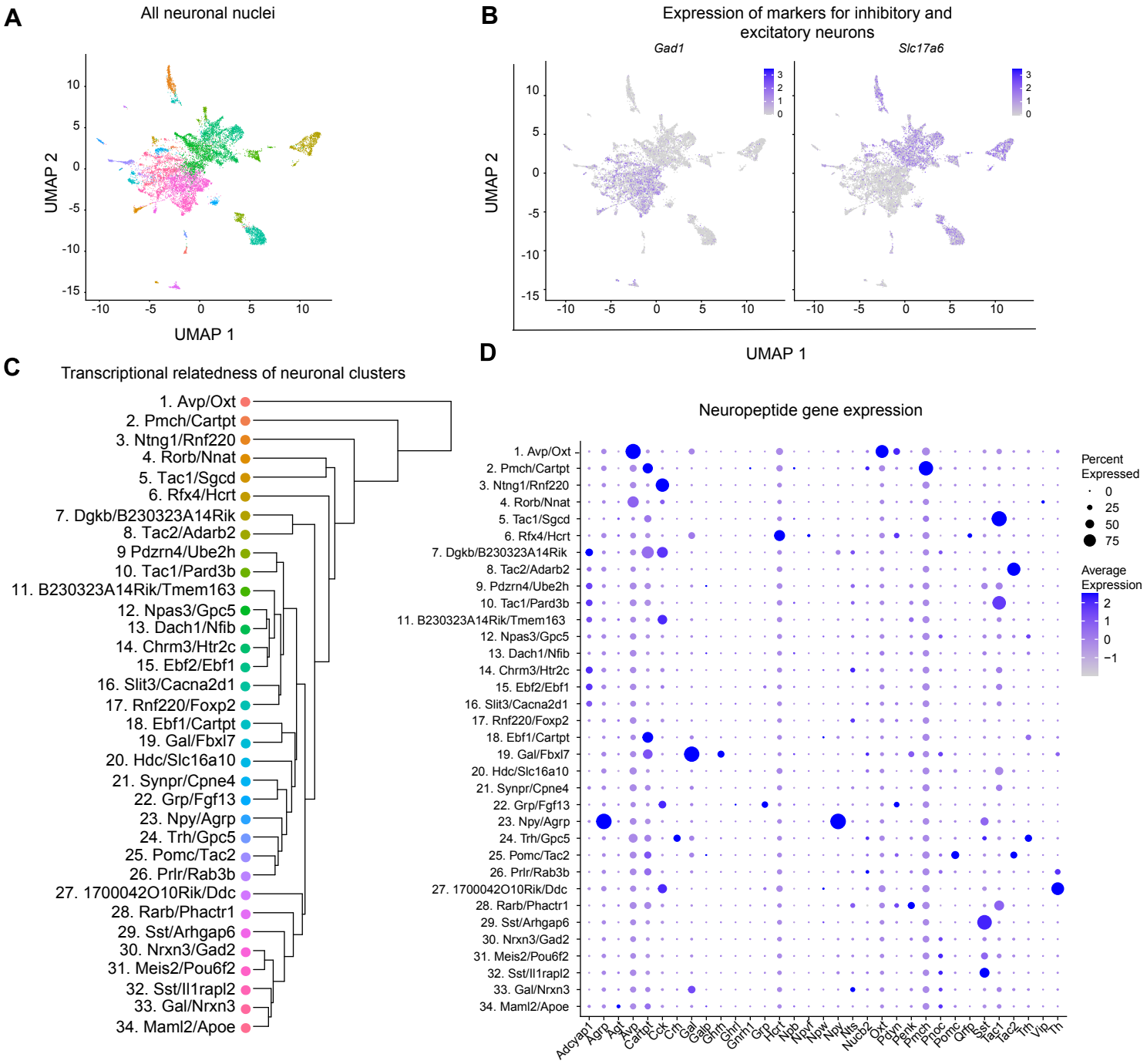
A
All neuronal nuclei
UMAP 2
UMAP 1
B
Expression of markers for inhibitory and excitatory neurons
Gad1
Slc17a6
UMAP 2
UMAP 1
C
Transcriptional relatedness of neuronal clusters
1. Avp/Oxt
2. Pmch/Cartpt
3. Ntng1/Rnf220
4. Rorb/Nnat
5. Tac1/Sgcd
6. Rfx4/Hcrt
7. Dgkb/B230323A14Rik
8. Tac2/Adarb2
9 Pdzrn4/Ube2h
10. Tac1/Pard3b
11. B230323A14Rik/Tmem163
12. Npas3/Gpc5
13. Dach1/Nfib
14. Chrm3/Htr2c
15. Ebf2/Ebf1
16. Slit3/Cacna2d1
17. Rnf220/Foxp2
18. Ebf1/Cartpt
19. Gal/Fbxl7
20. Hdc/Slc16a10
21. Synpr/Cpne4
22. Grp/Fgf13
23. Npy/Agrp
24. Trh/Gpc5
25. Pomc/Tac2
26. Prlr/Rab3b
27. 1700042O10Rik/Ddc
28. Rarb/Phactr1
29. Sst/Arhgap6
30. Nrxn3/Gad2
31. Meis2/Pou6f2
32. Sst/Il1rapl2
33. Gal/Nrxn3
34. Maml2/Apoe
D
Neuropeptide gene expression
Percent Expressed
Average Expression
Adcyap1 Agrp Agt Avp Cartpt Cck Crh Gal Galp Ghrh Ghrl Gnrh1 Grp Hcrt Npb Nppf Npw Npy Nts Nucb2 Oxt Pdyn Penk Pmch Pnoc Pomc Qrfp Sst Tac1 Tac2 Trh Vip Tn
E
Regulons for cell identity
23. Npy/Agrp
Tbx3
Polr3g
Stat3
Fli1
Erf
25. Pomc/Tac2
Stat5a
Nr5a2
Stat3
Ovol2
Gtf2f1

741 **Figure 6. Identification of transcriptionally distinct neuronal subtypes.** A) UMAP of all
742 neuronal nuclei. Distinct clusters are identified by color, with identities listed in (C). B)
743 FeaturePlots highlighting glutamatergic (*Slc17a6*) and GABAergic (*Gad1*) cell neuronal clusters.
744 Color scale indicates expression level. C) Neuronal clusters are labeled according to the top 2
745 marker genes and ordered based on overall transcriptional similarity. D) Expression of
746 neuropeptide genes in each cluster. Dot size indicates percent of nuclei expressing the gene,
747 color indicates intensity of expression.
748
749
750
751
752
753
754
755
756
757
758
759
760
761
762

Figure 7.

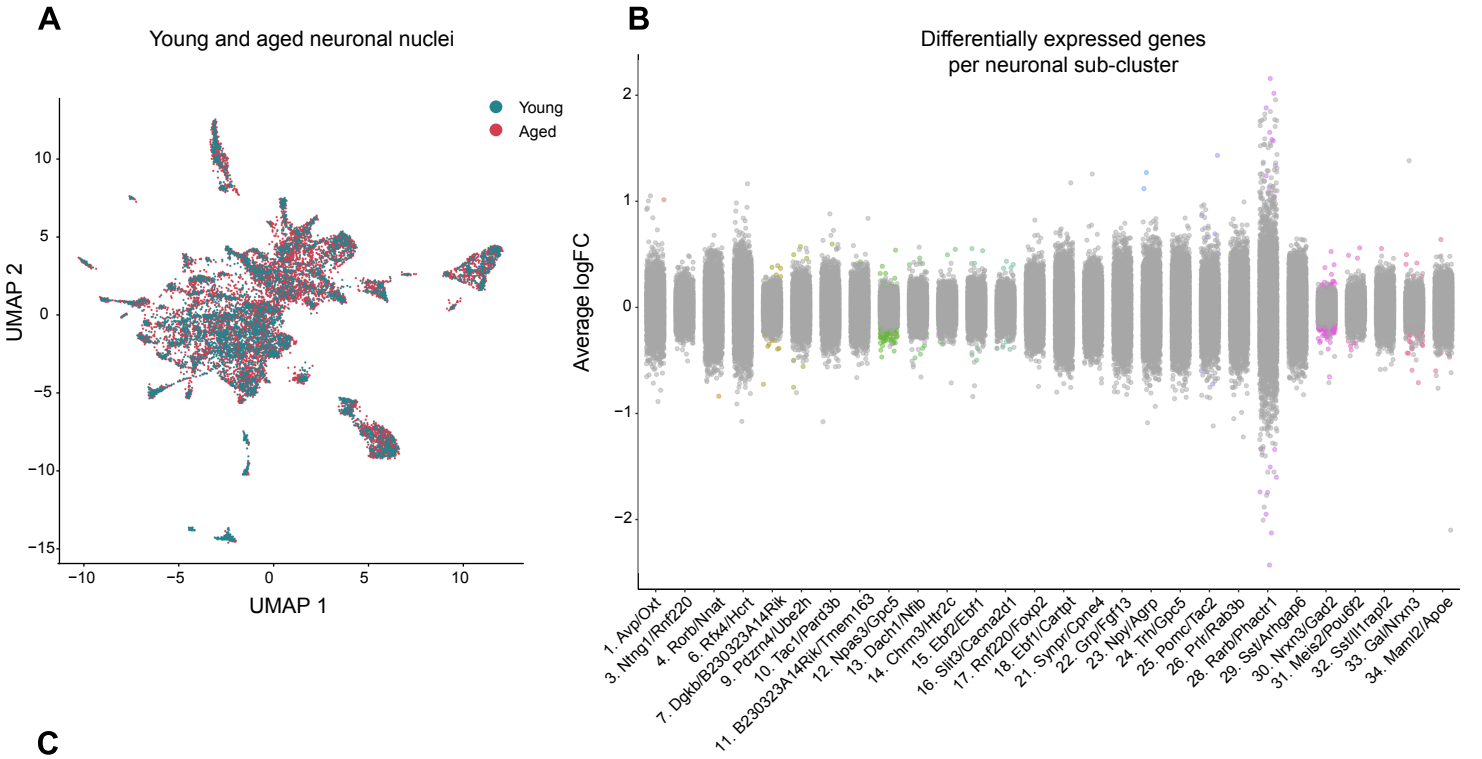
A
Young and aged neuronal nuclei
Young
Aged
UMAP 2
UMAP 1
B
Differentially expressed genes
per neuronal sub-cluster
Average logFC
1. Avp/Oxt
3. Ntng1/Rnf220
4. Rorb/Nnat
6. Rfx4/Hcrt
7. Dgkb/B230323A14Rik
9. Pdzrn4/Ube2h
10. Tac1/Pard3b
11. B230323A14Rik/Tmem163
12. Npas3/Gpc5
13. Dach1/Nfib
14. Chrm3/Htr2c
15. Ebf2/Ebf1
16. Slit3/Cacna2d1
17. Rnf220/Foxp2
18. Ebf1/Cartpt
21. Synpr/Cpne4
22. Grp/Fgf13
23. Npy/Agrp
24. Trh/Gpc5
25. Pomc/Tac2
26. Prlr/Rab3b
28. Rarb/Phactr1
29. Sst/Arhgap6
30. Nrxn3/Gad2
31. Meis2/Pou6f2
32. Sst/Il1rapl2
33. Gal/Nrxn3
34. Maml2/Apoe

C
Hallmark gene set enrichment analysis
NES
1. Avp/Oxt
3. Ntng1/Rnf220
4. Rorb/Nnat
6. Rfx4/Hcrt
7. Dgkb/B230323A14Rik
9. Pdzrn4/Ube2h
10. Tac1/Pard3b
11. B230323A14Rik/Tmem163
12. Npas3/Gpc5
13. Dach1/Nfib
14. Chrm3/Htr2c
15. Ebf2/Ebf1
16. Slit3/Cacna2d1
17. Rnf220/Foxp2
18. Ebf1/Cartpt
21. Synpr/Cpne4
22. Grp/Fgf13
23. Npy/Agrp
24. Trh/Gpc5
25. Pomc/Tac2
26. Prlr/Rab3b
28. Rarb/Phactr1
29. Sst/Arhgap6
30. Nrxn3/Gad2
31. Meis2/Pou6f2
32. Sst/Il1rapl2
33. Gal/Nrxn3
34. Maml2/Apoe
Osmoregulation/Social Behavior
Memory
Circadian rythym
Circadian rythym
Memory
Reproduction
Osmoregulation
Energy balance
Circadian rythym
Energy balance
Thermoregulation
Circadian rythym
Reproduction
Stress response
Growth
Growth
Adipogenesis
Cholesterol Homeostasis
DNA Repair
Estrogen Response Early
Estrogen Response Late
Fatty Acid Metabolism
Glycolysis
Hypoxia
Il2 Stat5 Signaling
Interferon Alpha Response
Interferon Gamma Response
KRAS Signaling Down
Mitotic Spindle
mTORC1 Signaling
MYC Targets V1
Myogenesis
Oxidative Phosphorylation
P53 Pathway
Peroxisome
ROS Pathway
Spermatogenesis
Unfolded Protein Response
UV Response Down
UV Response Up
Wnt Beta Catenin Signaling
Xenobiotic Metabolism

763 **Figure 7. Neuronal subtypes exhibit distinct transcriptional changes with age.** A) UMAP
764 plot of young and aged nuclei. B) Strip plot showing DE genes per cluster. Significant genes (FC
765 > 0.1, padj < 0.05) are colored, non-significant genes in gray. C) Heatmap of GSEA results for
766 each neuronal cluster. Significantly enriched terms (padj <0.1) are colored according to the
767 normalized enrichment score.
768
769
770
771
772
773
774
775
776
777
778
779
780
781
782
783
784

Supplementary Figure 1.

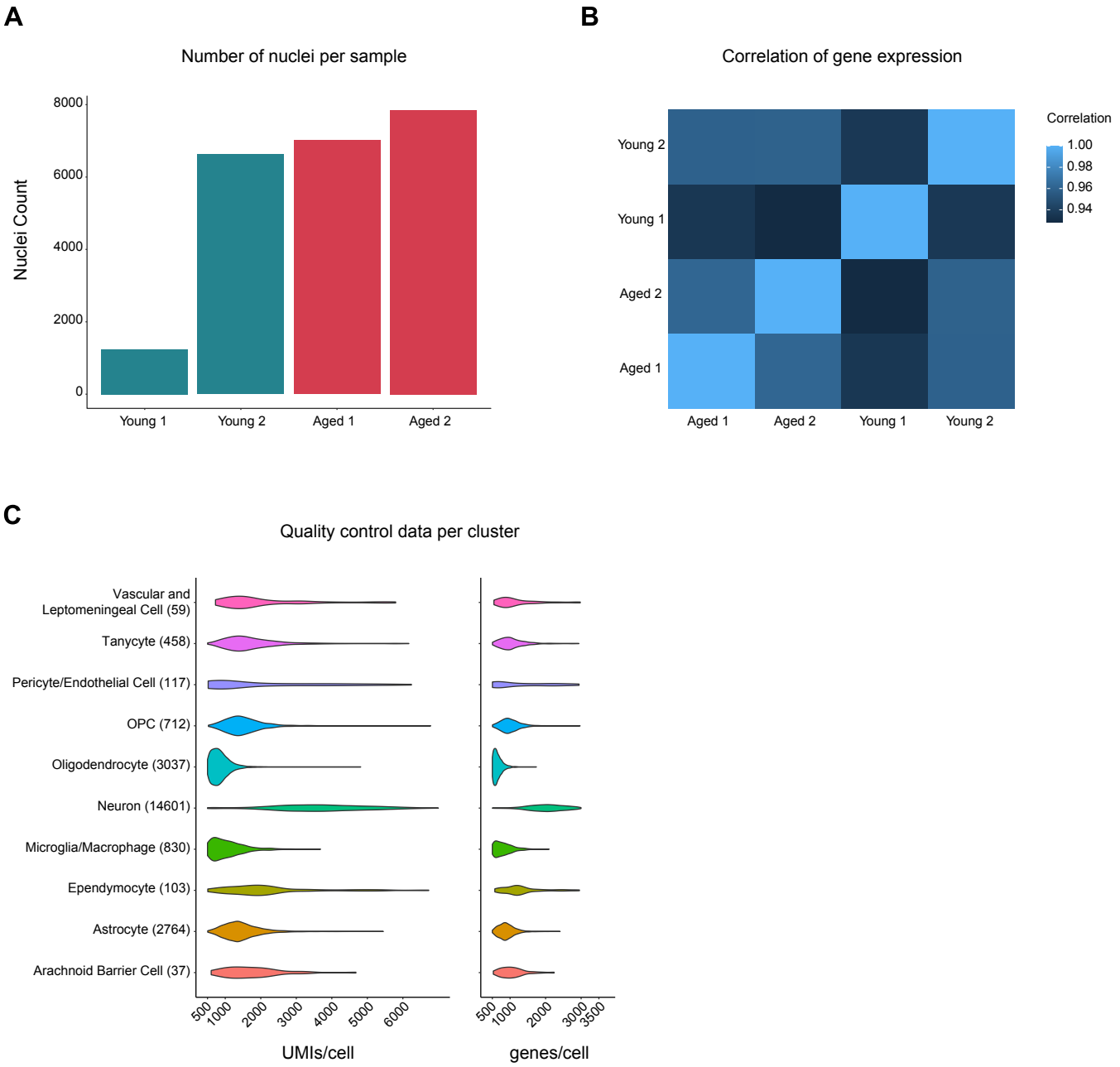

785 **Supplementary Figure 1**. Quality control metrics for single nuclei data. A) Number of nuclei
786 per sample. B) Correlation of gene expression (scaled) between each sample. Color reports
787 Spearman's correlation. C) Violin plots showing the number of UMIs per nuclei per cluster (left)
788 and the number of genes nuclei per cluster (right). Number of nuclei per cluster are listed in
789 parentheses.
790
791
792
793
794
795
796
797
798
799
800
801
802
803
804
805
806

Supplementary Figure 2.

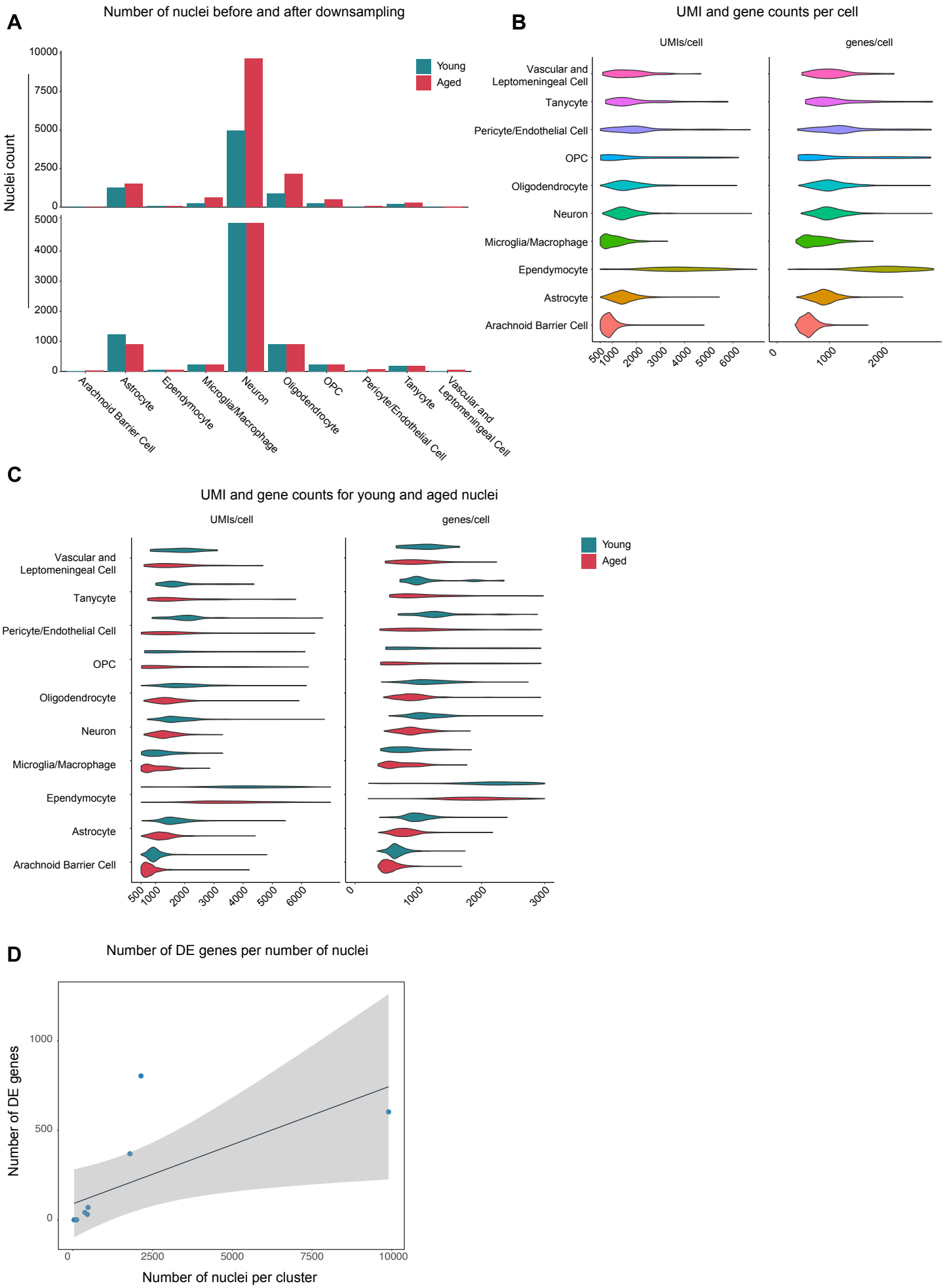

807 **Supplementary Figure 2.** Downsampling and quality control for downsampled clusters. A)
808 Number of nuclei per cell type before (top) and after (bottom) down sampling. B) Quality control
809 data for the nuclei used for analysis after down sampling. C) Quality control data after down
810 sampling split by age. D) Relationship between number of nuclei per cluster and the number of
811 differentially expressed genes. ($R2 = 0.510$, $p < 0.05$).
812
813

494 **REFERENCES**

495 1. Partridge, L., Deelen, J. & Slagboom, P. E. Facing up to the global challenges of ageing.
496 *Nature* **561**, 45–56 (2018).
497 2. Yousufuddin, M. & Young, N. Aging and ischemic stroke. *Aging* **11**, 2542–2544 (2019).
498 3. Balducci, L. & Aapro, M. Epidemiology of Cancer and Aging. in *Biological Basis of*
499 *Geriatric Oncology* 1–15 (Springer US, 2005).
500 4. Farooqui, T. & Farooqui, A. A. Aging: An important factor for the pathogenesis of
501 neurodegenerative diseases. *Mech. Ageing Dev.* **130**, 203–215 (2009).
502 5. Chahal, H. & Drake, W. The endocrine system and ageing. *J. Pathol.* **211**, 173–180 (2007).
503 6. Leibowitz, S. F. & Wortley, K. E. Hypothalamic control of energy balance: different
504 peptides, different functions. *Peptides* **25**, 473–504 (2004).
505 7. Hiller-Sturmhöfel, S. & Bartke, A. The Endocrine System. *Alcohol Health Res. World* **22**,
506 153–164 (1998).
507 8. de Cabo, R., Carmona-Gutierrez, D., Bernier, M., Hall, M. N. & Madeo, F. The Search for
508 Antiaging Interventions: From Elixirs to Fasting Regimens. *Cell* **157**, 1515–1526 (2014).
509 9. Bishop, N. A. & Guarente, L. Two neurons mediate diet-restriction-induced longevity in C.
510 elegans. *Nature* **447**, 545–549 (2007).
511 10. Broughton, S. J. *et al.* DILP-producing Median Neurosecretory Cells in the Drosophila Brain
512 Mediate the Response of Lifespan to Dietary Restriction. *Aging Cell* **9**, 336–346 (2010).
513 11. Satoh, A. *et al.* Sirt1 extends life span and delays aging in mice through the regulation of
514 Nk2 homeobox 1 in the DMH and LH. *Cell Metab.* **18**, 416–430 (2013).
515 12. Zhang, G. *et al.* Hypothalamic programming of systemic ageing involving IKK-β, NF-κB
516 and GnRH. *Nature* **497**, 211–216 (2013).

517 13. Ximerakis, M. *et al.* Single-cell transcriptomic profiling of the aging mouse brain. *Nat.*
518 *Neurosci.* **22**, 1696–1708 (2019).
519 14. Benayoun, B. A. *et al.* Remodeling of epigenome and transcriptome landscapes with aging in
520 mice reveals widespread induction of inflammatory responses. *Genome Res.* **29**, 697–709
521 (2019).
522 15. Webb, A. E., Kundaje, A. & Brunet, A. Characterization of the direct targets of FOXO
523 transcription factors throughout evolution. *Aging Cell* **15**, 673–685 (2016).
524 16. Hofmann, J. W. *et al.* Reduced Expression of MYC Increases Longevity and Enhances
525 Healthspan. *Cell* **160**, 477–488 (2015).
526 17. Chen, R., Wu, X., Jiang, L. & Zhang, Y. Single-Cell RNA-Seq Reveals Hypothalamic Cell
527 Diversity. *Cell Rep.* **18**, 3227–3241 (2017).
528 18. Mickelsen, L. E. *et al.* Single-cell transcriptomic analysis of the lateral hypothalamic area
529 reveals molecularly distinct populations of inhibitory and excitatory neurons. *Nat. Neurosci.*
530 **22**, 642–656 (2019).
531 19. Wen, S. *et al.* Spatiotemporal single-cell analysis of gene expression in the mouse
532 suprachiasmatic nucleus. *Nat. Neurosci.* **23**, 456–467 (2020).
533 20. Moffitt, J. R. *et al.* Molecular, spatial, and functional single-cell profiling of the
534 hypothalamic preoptic region. *Science* **362**, eaau5324 (2018).
535 21. Campbell, J. N. *et al.* A Molecular Census of Arcuate Hypothalamus and Median Eminence
536 Cell Types. *Nat. Neurosci.* **20**, 484–496 (2017).
537 22. Bakken, T. E. *et al.* Single-nucleus and single-cell transcriptomes compared in matched
538 cortical cell types. *PLOS ONE* **13**, (2018).

539 23. Ding, J. *et al.* Systematic comparison of single-cell and single-nucleus RNA-sequencing
540 methods. *Nat. Biotechnol.* **38**, 737–746 (2020).
541 24. Van de Sande, B. *et al.* A scalable SCENIC workflow for single-cell gene regulatory
542 network analysis. *Nat. Protoc.* **15**, 2247–2276 (2020).
543 25. Goodman, T. & Hajihosseini, M. K. Hypothalamic tanycytes—masters and servants of
544 metabolic, neuroendocrine, and neurogenic functions. *Front. Neurosci.* **9**, (2015).
545 26. Lee, D. A. *et al.* Tanycytes of the hypothalamic median eminence form a diet-responsive
546 neurogenic niche. *Nat. Neurosci.* **15**, 700–702 (2012).
547 27. Webb, A. E. *et al.* FOXO3 Shares Common Targets with ASCL1 Genome-wide and Inhibits
548 ASCL1-Dependent Neurogenesis. *Cell Rep.* **4**, 477–491 (2013).
549 28. Finak, G. *et al.* MAST: a flexible statistical framework for assessing transcriptional changes
550 and characterizing heterogeneity in single-cell RNA sequencing data. *Genome Biol.* **16**, 278
551 (2015).
552 29. Stuart, T. *et al.* Comprehensive Integration of Single-Cell Data. *Cell* **177**, 1888-1902.e21
553 (2019).
554 30. Roberts, S. B. & Rosenberg, I. Nutrition and Aging: Changes in the Regulation of Energy
555 Metabolism With Aging. *Physiol. Rev.* **86**, 651–667 (2006).
556 31. Brockdorff, N. & Duthie, S. M. X chromosome inactivation and the Xist gene. *Cell. Mol.*
557 *Life Sci. CMLS* **54**, 104–112 (1998).
558 32. Lee, J. T., Davidow, L. S. & Warshawsky, D. Tsix, a gene antisense to Xist at the X-
559 inactivation centre. *Nat. Genet.* **21**, 400–404 (1999).
560 33. Liberzon, A. *et al.* The Molecular Signatures Database (MSigDB) hallmark gene set
561 collection. *Cell Syst.* **1**, 417–425 (2015).

562 34. Luo, X.-G., Ding, J.-Q. & Chen, S.-D. Microglia in the aging brain: relevance to
563 neurodegeneration. *Mol. Neurodegener.* **5**, 12 (2010).
564 35. Trapnell, C. *et al.* The dynamics and regulators of cell fate decisions are revealed by
565 pseudotemporal ordering of single cells. *Nat. Biotechnol.* **32**, 381–386 (2014).
566 36. Lemaître, J.-F. *et al.* Sex differences in adult lifespan and aging rates of mortality across wild
567 mammals. *Proc. Natl. Acad. Sci. U. S. A.* **117**, 8546–8553 (2020).
568 37. Mitchell, S. J. *et al.* Effects of Sex, Strain, and Energy Intake on Hallmarks of Aging in
569 Mice. *Cell Metab.* **23**, 1093–1112 (2016).
570 38. Kane, A. E., Sinclair, D. A., Mitchell, J. R. & Mitchell, S. J. Sex differences in the response
571 to dietary restriction in rodents. *Curr. Opin. Physiol.* **6**, 28–34 (2018).
572 39. Willard, H. F. & Carrel, L. Making sense (and antisense) of the X inactivation center. *Proc.*
573 *Natl. Acad. Sci.* **98**, 10025–10027 (2001).
574 40. Chureau, C. *et al.* Ftx is a non-coding RNA which affects Xist expression and chromatin
575 structure within the X-inactivation center region. *Hum. Mol. Genet.* **20**, 705–718 (2011).
576 41. Berletch, J. B. *et al.* Escape from X Inactivation Varies in Mouse Tissues. *PLoS Genet.* **11**,
577 (2015).
578 42. Sternson, S. M. Hypothalamic Survival Circuits: Blueprints for Purposive Behaviors. *Neuron*
579 **77**, 810–824 (2013).
580 43. Toda, C., Santoro, A., Kim, J. D. & Diano, S. POMC Neurons: From Birth to Death. *Annu.*
581 *Rev. Physiol.* **79**, 209–236 (2017).
582 44. Ma, T., Wong, S. Z. H., Lee, B., Ming, G. & Song, H. Decoding neuronal composition and
583 ontogeny of individual hypothalamic nuclei. *Neuron* (2021).

584 45. Vann, S. D. & Nelson, A. J. D. The mammillary bodies and memory. in *Progress in Brain*
585 *Research* vol. 219 163–185 (Elsevier, 2015).
586 46. Işıldak, U., Somel, M., Thornton, J. M. & Dönertaş, H. M. Temporal changes in the gene
587 expression heterogeneity during brain development and aging. *Sci. Rep.* **10**, 4080 (2020).
588 47. López-Otín, C., Blasco, M. A., Partridge, L., Serrano, M. & Kroemer, G. The Hallmarks of
589 Aging. *Cell* **153**, 1194–1217 (2013).
590 48. Leng, K. *et al.* Molecular characterization of selectively vulnerable neurons in Alzheimer's
591 disease. *Nat. Neurosci.* **24**, 276–287 (2021).
592 49. Krashes, M. J. *et al.* Rapid, reversible activation of AgRP neurons drives feeding behavior in
593 mice. *J. Clin. Invest.* **121**, 1424–1428 (2011).
594 50. Williams, K. W. *et al.* Xbp1s in Pomc Neurons Connects ER Stress with Energy Balance and
595 Glucose Homeostasis. *Cell Metab.* **20**, 471–482 (2014).
596 51. Austad, S. N. Why women live longer than men: Sex differences in longevity. *Gend. Med.* **3**,
597 79–92 (2006).
598 52. Sampathkumar, N. K. *et al.* Widespread sex dimorphism in aging and age-related diseases.
599 *Hum. Genet.* **139**, 333–356 (2020).
600 53. Costs of sexual selection in natural populations of mammals. *Proc. R. Soc. Lond. B Biol. Sci.*
601 **247**, 203–210 (1992).
602 54. Burger, J. M. S. Sex-Specific Effects of Interventions That Extend Fly Life Span. *Sci. Aging*
603 *Knowl. Environ.* **28**, 30 (2004).
604 55. Honjoh, S., Ihara, A., Kajiwara, Y., Yamamoto, T. & Nishida, E. The Sexual Dimorphism of
605 Dietary Restriction Responsiveness in Caenorhabditis elegans. *Cell Rep.* **21**, 3646–3652
606 (2017).

607 56. Davis, E. J., Lobach, I. & Dubal, D. B. Female XX sex chromosomes increase survival and
608 extend lifespan in aging mice. *Aging Cell* **18**, e12871 (2019).
609 57. Sergushichev, A. A. An algorithm for fast preranked gene set enrichment analysis using
610 cumulative statistic calculation. *bioRxiv* 060012 (2016) doi:10.1101/060012.
611 58. Wouters, J. *et al.* Robust gene expression programs underlie recurrent cell states and
612 phenotype switching in melanoma. *Nat. Cell Biol.* **22**, 986–998 (2020).
613 59. Suo, S. *et al.* Revealing the Critical Regulators of Cell Identity in the Mouse Cell Atlas. *Cell*
614 *Rep.* **25**, 1436-1445.e3 (2018).
615
616
617
618
619
620
621
622
623
624
625
626
627
628
629